npg

Reduction of endoplasmic reticulum Ca^{2+} levels favors plasma membrane surface exposure of calreticulin

R Tufi[1,2,3,4], T Panaretakis[1,2,3], K Bianchi[5], A Criollo[1,2,3], B Fazi[4], F Di Sano[4], A Tesniere[1,2,3], O Kepp[1,2,3], P Paterlini-Brechot[5], L Zitvogel[2,3,6], M Piacentini[4], G Szabadkai[5,7,8] and G Kroemer*[,1,2,3,8]

Some chemotherapeutic agents can elicit apoptotic cancer cell death, thereby activating an anticancer immune response that influences therapeutic outcome. We previously reported that anthracyclins are particularly efficient in inducing immunogenic cell death, correlating with the pre-apoptotic exposure of calreticulin (CRT) on the plasma membrane surface of anthracyclin-treated tumor cells. Here, we investigated the role of cellular Ca^{2+} homeostasis on CRT exposure. A neuroblastoma cell line (SH-SY5Y) failed to expose CRT in response to anthracyclin treatment. This defect in CRT exposure could be overcome by the overexpression of Reticulon-1C, a manipulation that led to a decrease in the Ca^{2+} concentration within the endoplasmic reticulum lumen. The combination of Reticulon-1C expression and anthracyclin treatment yielded more pronounced endoplasmic reticulum Ca^{2+} depletion than either of the two manipulations alone. Chelation of intracellular (and endoplasmic reticulum) Ca^{2+}, targeted expression of the ligand-binding domain of the IP_3 receptor and inhibition of the sarco-endoplasmic reticulum Ca^{2+}-ATPase pump reduced endoplasmic reticulum Ca^{2+} load and promoted pre-apoptotic CRT exposure on the cell surface, in SH-SY5Y and HeLa cells. These results provide evidence that endoplasmic reticulum Ca^{2+} levels control the exposure of CRT.
Cell Death and Differentiation (2008) **15,** 274–282; doi:10.1038/sj.cdd.4402275; published online 23 November 2007

In contrast to prior belief, apoptotic cell death can be immunogenic and hence elicits an active immune response against dying tumor cells.[1] This is therapeutically relevant because immune defects that compromise the response against apoptotic cells reduce the efficacy of anticancer chemotherapy, both in suitable animal models and in patients.[2] We found that anthracyclins and γ-irradiation are particularly efficient in inducing immunogenic cell death, at least in mouse models.[3–5] The immunogenicity of cellular demise correlates with the exposure of calreticulin (CRT) on the plasma membrane (PM) surface of stressed tumor cells, a phenomenon that manifests before the cells acquire signs of apoptosis such as phosphatidylserine exposure. Inhibition of CRT exposure curtails the capacity of anthracyclin-treated or irradiated tumor cells to vaccinate against cancer and reduces the therapeutic efficacy of anthracyclins on tumors established in immunocompetent hosts.[3–5] Provision of recombinant CRT or drug-mediated enforcement of CRT exposure rendered *per se* nonimmunogenic chemotherapies (for instance with etoposide and mitomycin C) immunogenic and

boosted their therapeutic efficacy.[5] These results suggest that CRT exposure is both necessary and sufficient to render conventional chemotherapies immunogenic.

CRT is an abundant Ca^{2+}-binding chaperone that is mostly present in the endoplasmic reticulum (ER) lumen, although it can also be found in other subcellular localizations.[6,7] When present on the surface of damaged cells, it can serve as an 'eat-me' signal and hence facilitate the recognition and later engulfment of the dying cells by macrophages[8] or by dendritic cells.[5] It is thought that this function determines the immunostimulatory effect of CRT, because presentation of tumor antigens by dendritic cells is indeed required for the immunogenic effect of anthracyclin-treated cancer cells.[1,5,9] Alternatively or in addition, CRT may bind antigenic peptides from the tumor and facilitate their efficient presentation to T cells.[10]

The exposure of CRT on the cell surface induced by anthracyclins has been found to involve the translocation of pre-synthetized CRT, through an active process that relies on the activity of the actin cytoskeleton.[2] It occurs within minutes

[1]INSERM, U848, Villejuif F-94805, France; [2]Institut Gustave Roussy, Villejuif F-94805, France; [3]University Paris-Sud, Paris 11, Villejuif F-94805, France; [4]Department of Biology, University of Tor Vergata, Rome I-00133, Italy; [5]INSERM U807, University Paris V, Faculty of Medicine, Hospital Necker-Enfants Malades, Paris F-75015, France; [6]INSERM, U805, Villejuif F-94805, France and [7]Department of Physiology, University College London, Gower Street, London WC1E 6BT, UK
*Corresponding author: G Kroemer, INSERM, U848, Institut Gustave Roussy, Pavillon de Recherche 1, 39 rue Camille-Desmoulins, Villejuif F-94805, France.
Tel: + 33 1 42 11 60 46; Fax: + 33 1 42 11 60 47; E-mail: kroemer@igr.fr
[8]These authors share senior co-authorship.

after addition of the anthracyclin and does not involve a general mixing of the ER membrane with the PM, as indicated by the fact that the ER transmembrane protein calcineurin (a close CRT homolog) is not found on the cell surface.[5] This is at difference with the reported mixing of intracellular membranes from the Golgi apparatus with the PM, which occurs at late-stage apoptosis concomitant with membrane blebbing.[11,12]

Importantly, it has been found that cytoplasts (that is cells lacking a nucleus) were still able to expose CRT on the cell surface when they were treated with anthracyclins.[5] This result indicates that anthracyclins induce CRT exposure through a non-nuclear, cytoplasmic effect. Thus, the anthracyclin-stimulated CRT exposure is not mediated by a classical DNA damage response (which would involve the nucleus). Anthracyclins have been reported to exert a direct toxic effect on the PM,[13] to stimulate ceramide synthesis,[14] to induce the generation of reactive oxygen species,[15,16] and to affect intracellular Ca^{2+} homeostasis, mainly by reducing ER Ca^{2+} concentrations,[17,18] perhaps through a direct effect on ER proteins such as calsequestrin.[19]

Based on the aforementioned information, we decided to investigate the impact of ER Ca^{2+} homeostasis on the regulation of CRT exposure on the surface of anthracyclin-treated tumor cells. To this aim, we characterized a neuroblastoma cell line, demonstrating that it fails to expose CRT on the surface upon treatment with anthracyclins, yet recovers this capacity after expression of a tetracycline-inducible reticulon-1C (RTN-1C) transgene, correlating with a reduced ER Ca^{2+} level. In addition, we used an extensive repertoire of pharmacological and genetic manipulations of the ER Ca^{2+} influx and efflux to document that a reduction of ER Ca^{2+} concentrations can favor the translocation of CRT to the cell surface.

Results and Discussion

Establishment and characterization of human neuroblastoma cells expressing inducible RTN-1C. Reticulons (RTNs) are evolutionary conserved proteins that are differentially expressed in different cell types.[20–22] RTNs localize primarily to the ER membrane and possess unique N-terminal parts and a common 200-amino-acid C-terminal domain containing two long hydrophobic sequences that were suggested to form Ca^{2+}-permeable pores in the ER membrane.[23–25] RTN-1C represents the smallest variant of the reticulon 1 gene[26] and it is specifically expressed by neurons and cells of neuroendocrine tissue.[27] In our study, we used the previously developed tetracycline-inducible SH-SY5Y^{RTN-1C} human neuroblastoma model[23] consisting of a SH-SY5Y cell line stably expressing tetracycline-inducible RTN-1C (SH-SY5Y^{RTN-1C}) and a control cell line expressing the regulator vector alone (SH-SY5Y^{Tet12}) (Figure 1a). After addition of doxycycline, a tetracycline derivative, SH-SY5Y^{RTN-1C} cells overexpress RTN-1C within hours, reaching a peak around 6 h that remains constant for several days (Figure 1b). While most of the RTN-1C is present on intracellular membranes ('Endo-RTN-1C') (Figure 1c), some of it can also be detected on the PM surface ('Ecto-RTN-1C')
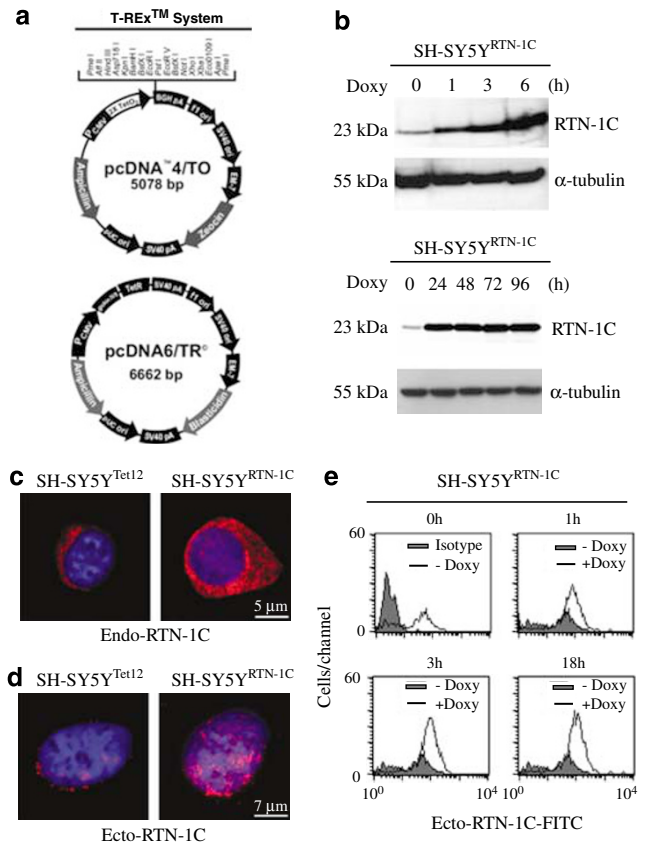

Figure 1 Characterization of SH-SY5Y neuroblastoma cells expressing tetracycline-inducible RTN-1C. (**a**) Plasmid maps. The two components of the tetracycline-regulated mammalian expression system (Invitrogen's T-REx™ System) used to develop the SH-SY5Y^{RTN-1C} tetracycline inducible cell line are shown. On the top, the pcDNA™4/TO expression vector with the two tetracycline operator sequences (TetO$_2$); on the bottom, the pcDNA™6/TR regulatory vector providing high-level expression of the tetracycline repressor (TR) protein and present in the SH-SY5Y^{Tet12} control cell line. (**b**) Analysis of RTN-1C expression in stable RTN-1C-expressing clone generated from SH-SY5Y$^{tet/on}$ cells. Western blot analysis of RTN-1C in SH-SY5Y^{RTN-1C} cells, treated with 2 μg/ml doxycycline for different times. The protein is strongly upregulated as soon as 1 h of induction (top panel) and this increase is maintained to 96 h of treatment (lower panel). (**c**) Intracellular and (**d**) cell surface RTN-1C staining for the detection of endo-CRT and ecto-CRT, respectively, in SH-SY5Y^{Tet12} and SH-SY5Y^{RTN-1C} treated with 2 μg/ml doxycycline for 12 h. (**e**) Cytofluorometric detection of ecto-RTN-1C in SH-SY5Y^{RTN-1C} cells. Non-doxycycline-induced SH-SY5Y^{RTN-1C} cells (−doxy) were harvested at the same time of the 18 h doxycycline-treated cells. The immunodetection of the RTN-1C protein on the cell surface was analyzed at different times of 2 μg/ml doxycycline induction by flow cytometry using an anti-FITC conjugated antibody as described in 'Materials and Methods' section

by immunofluorescence staining of nonpermeabilized cells, either by digital imaging (Figure 1d) or cytofluorometric detection (Figure 1e). We have previously observed that RTN-1C-overexpressing cells (that is SH-SY5Y^{RTN-1C} treated with doxycycline) are relatively resistant against DNA-damaging agents such as etoposide or cisplatin, as compared to controls (SH-SY5Y^{Tet12} or SH-SY5Y^{RTN-1C} cells cultured in tetracycline-free conditions).[23] In contrast, we found that the overexpression of RTN-1C had no effect on the propensity of cells to expose phosphatidylserine and to lose viability (Figure 2a and b) or to activate caspase-3 (Figure 2c) after treatment with the anthracyclin mitoxanthrone (MITO).
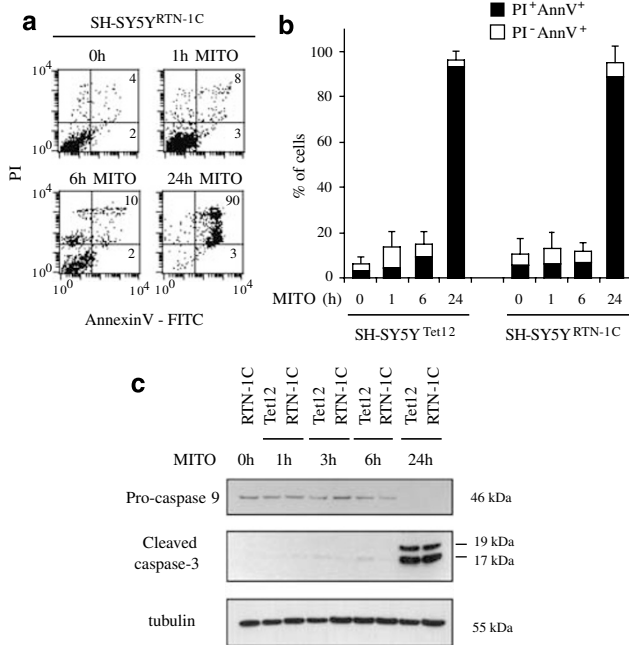
Figure 2 Apoptotic response of SH-SY5Y^{Tet12} and SH-SY5Y^{RTN-1C} to MITO treatment. (**a**) Representative FACS pictograms of cells that were treated with 1 μM MITO for different times and then stained with annexinV-FITC and PI and analyzed by flow cytometry. Percentages of annexinV-positive and PI-negative cells (apoptotic cells, lower right quadrant) and annexinV/PI-double-positive cells (necrotic cells, upper right quadrant) are indicated. (**b**) Quantitative analysis of annexinV-FITC and PI staining at different times of 1 μM MITO. Results are means of triplicates ± S.E.M. Similar results were obtained in three independent experiments. (**c**) Western blot analysis of caspase activation in MITO-treated neuroblastoma cells. SH-SY5Y^{Tet12} and SH-SY5Y^{RTN-1C} cells were treated with 1 μM MITO for the indicated times and equal amounts of total proteins were subjected to immunoblot detection of pro-caspase 9 (46 kDa) and cleaved caspase-3 (17, 19 kDa). Tubulin was used as a loading control

RTN-1C facilitates CRT exposure in response to anthracyclin treatment. When MITO was added to doxycycline-treated SH-SY5Y^{Tet12}, no increase in the expression of ecto-CRT could be detected. Thus, the level of ecto-CRT, as detectable by immunofluorescence staining and subsequent cytofluorometric analysis, did not increase in MITO-treated SH-SY5Y^{Tet12} cells (Figure 3a, top panels). In marked contrast, we found that SH-SY5Y^{RTN-1C} neuroblastoma cells cultured in the presence of MITO did manifest an increase in the ecto-CRT level, as detectable by flow cytometry as soon as 30 or 120 min after addition of MITO (Figure 3a, bottom panels). It should be noted that neither SH-SY5Y^{Tet12} nor SH-SY5Y^{RTN-1C} cells did manifest any signs of apoptosis at these time points (Figure 2a and b), meaning that the MITO-induced ecto-CRT exposure is an early event. MITO-triggered ecto-CRT exposure is a pre-apoptotic feature in the sense that it is found on cells that still lack phosphatidylserine exposure. Later, after 24 h of stimulation, MITO induced *bona fide* apoptosis, exactly as in mouse colon cancer and fibrosarcoma cells,[1] as indicated by chromatin condensation (not shown) and caspase activation (Figure 2c). MITO did not induce an increase in total CRT levels, as determined by immunoblot analysis (Figure 3b), suggesting that ecto-CRT exposure is due to the redistribution rather than *de novo* synthesis of CRT. The increase in ecto-CRT on the surface of doxycycline-pretreated and MITO-treated SH-SY5Y^{RTN-1C} cells could also be detected by *in situ* immunofluorescence staining, revealing a patchy distribution of ecto-CRT, usually only in one single area of the PM (Figure 3c). While there was some background staining in control cells, we consistently found an increase in ecto-CRT when the overexpression of RTN-1C was combined with MITO treatment. Although ecto-CRT colocalized with ecto-RTN-1C in the same area of the cell surface (Figure 3d), we failed to co-immunoprecipitate CRT and RTN-1C either before or after MITO treatment (not shown). Accordingly, the subcellular localization of endo-CRT and endo-RTN-1C only partially overlapped, as determined by confocal imaging of permeabilized cells (Supplementary Figure 1). As an internal control, brefeldin A (BFA) fully blocked the ecto-CRT exposure induced by MITO in RTN-1C-overexpressing cells (Figure 4a), causing a perinuclear accumulation of endo-CRT and endo-RTN-1C (Figure 4b). This indicates that the anthracyclin-induced translocation of CRT from the ER to the cell surface is not due to passive leakage of the protein from the lumen of the ER, suggesting that it is plausibly an active process.

Altogether, these results indicate that RTN-1C can facilitate the active translocation of pre-formed CRT from the cytoplasm (endo-CRT) to the cell surface (ecto-CRT).

RTN-1C and MITO reduce ER luminal [Ca^{2+}] in a concerted manner. In order to determine the effect of RTN-1C overexpression on ER Ca^{2+} homeostasis, SH-SY5Y^{RTN-1C} cells were infected with an adenoviral construct encoding ER-targeted low-affinity aequorin probe (ad-er-AEQ), and RTN-1C induction was achieved by the addition of doxycycline as detailed above (see Figure 1b).

The steady-state concentration of Ca^{2+} in the ER lumen ([Ca^{2+}]$_{ER}$) varies between 200 and 800 μM, depending on the cell type and the state of the cell, and is determined by the balance between Ca^{2+} accumulation into and Ca^{2+} release from the organelle. In the last decade, several methods have been developed for dynamic assessment of [Ca^{2+}]$_{ER}$ in living cells.[28] The aequorin-based measurement, applied in our study, is based on a protocol which includes (i) pre-incubation of cells with the aequorin cofactor coelenterazine n, following complete Ca^{2+} depletion of the ER in Ca^{2+}-free medium; (ii) refilling of the ER by addition of 1 mM CaCl$_2$ to the extracellular medium until [Ca^{2+}] in the ER lumen ([Ca^{2+}]$_{ER}$) reaches steady state; and (iii) release of Ca^{2+} through Ca^{2+} leak or release channels[29,30] (see also Materials and Methods). The strategic advantage of this protocol was that it allowed us to analyze separately the three fundamental parameters of ER Ca^{2+} homeostasis, respectively: (i) Ca^{2+} accumulation into the ER, through the complex interplay between store-operated Ca^{2+} influx into the cell immediately followed by its transport into the ER lumen by sarcoendoplasmic reticulum Ca^{2+}-ATPase (SERCA);[31,32] (ii) steady-state ER luminal Ca^{2+} concentration ([Ca^{2+}]$_{ER}$) determining Ca^{2+}-dependent folding and redox processes of the organelle[33,34]; and (iii) the Ca^{2+} leak observed after inhibition of SERCA-mediated Ca^{2+} uptake by 2,5-di(t-butyl)-1,4-benzo-hydroquinone (tBHQ)[29] (Figure 5a). As shown on Figure 5a
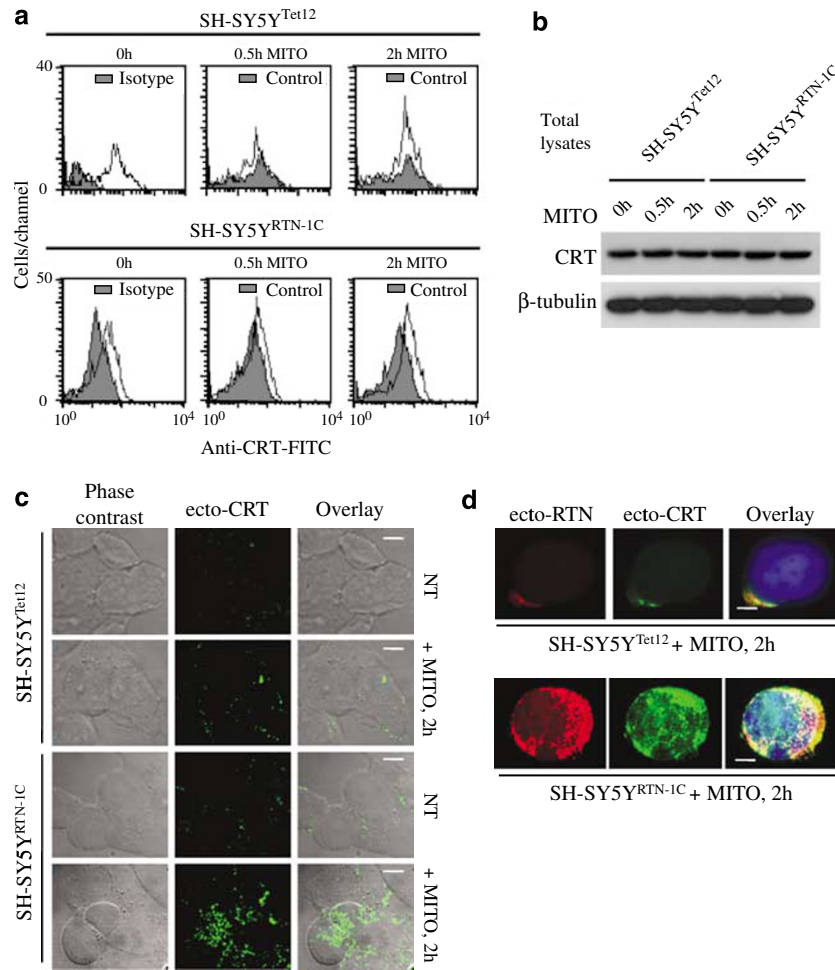
Figure 3 RTN-1C overexpression facilitates the exposure of CRT induced by MITO. (**a**) Cytofluorometric detection of CRT exposure. SH-SY5Y^{Tet12} and SH-SY5Y^{RTN-1C} were treated with 1 μM MITO for 0.5 or 2 h and the exposure of CRT was determined by immunofluorescence detection as described in Materials and Methods. (**b**) Immunoblot detection of total CRT levels. CRT was detected in total lysates from SH-SY5Y^{Tet12} and SH-SY5Y^{RTN-1C} treated with 1 μM MITO for the indicated time. β-tubulin was used as a loading control. (**c**) *In situ* immunofluorescence detection of CRT exposure. The presence of CRT on the cell surface (ecto-CRT) was detected in nonpermeabilized SH-SY5Y^{Tet12} and SH-SY5Y^{RTN-1C} cells after MITO treatment (2 h, 1 μM). CRT staining (green) and phase contrast images and their overlay are shown both in nontreated (NT) and MITO-treated cells. Scale bar = 10 μm. (**d**) Immunofluorescence detection of ecto-RTN-1C (red) and ecto-CRT (green) in SH-SY5Y^{Tet12} (upper panel) and SH-SY5Y^{RTN-1C} cells (lower panel) after 2 h of 1 μM MITO treatment. Nuclei are stained with DAPI (blue). Scale bar = 5 μm

and b (top panel), RTN-1C overexpression led to partial reduction of the steady-state $[Ca^{2+}]_{ER}$. This effect is in line with our previous report on a reduced carbachol-releasable Ca^{2+} pool and elevated basal cytoplasmic Ca^{2+} levels in SH-SY5Y^{RTN-1C} cells.[23] Moreover, our analysis revealed that the reduction of $[Ca^{2+}]_{ER}$ was, for the most part, the consequence of the significant inhibition of Ca^{2+} accumulation into the ER, following Ca^{2+} addition to the extracellular space (Figure 5b, middle panel). Even if the mean Ca^{2+} leak was increased, it did not reach a statistically significant level (Figure 5b, lower panel). Transient transfection of HeLa cells with RTN-1C also led to reduction of $[Ca^{2+}]_{ER}$ (Supplementary Figure 2).

Since RTN-1C facilitates CRT exposure in response to anthracyclin treatment (see Figure 3a and c), we decided to analyze the combined effect of MITO and RTN-1C over-expression on the above parameters of ER Ca^{2+} handling. MITO also reduced $[Ca^{2+}]_{ER}$, both in RTN-1C-overexpressing and in control cells (that is SH-SY5Y^{RTN-1C} cells cultured

in the presence or absence of doxycycline, respectively, Figure 5b, top panel). This effect of MITO involved (i) a major inhibition of the Ca^{2+} accumulation from the extracellular space into the ER lumen (Figure 5b middle panel), but (ii) also rendered the ER more leaky to Ca^{2+}, resulting in significant increase of Ca^{2+} loss following tBHQ addition (Figure 5b, lower panel). Altogether, the combination of RTN-1C over-expression and MITO treatment was particularly efficient in depleting $[Ca^{2+}]_{ER}$ levels, by combining a reduced Ca^{2+} accumulation and an enhanced Ca^{2+} efflux.

Reduction of ER Ca^{2+} load triggers CRT exposure. As shown above, RTN-1C and MITO both reduce $[Ca^{2+}]_{ER}$ levels and induce ecto-CRT. To causally link both phenomena, we sought to reduce $[Ca^{2+}]_{ER}$ by different techniques and to monitor the effect of these manipulations on CRT exposure. For this set of experiments, we utilized HeLa cells, allowing pharmacological treatment and transient overexpression of constructs interacting with the ER Ca^{2+}
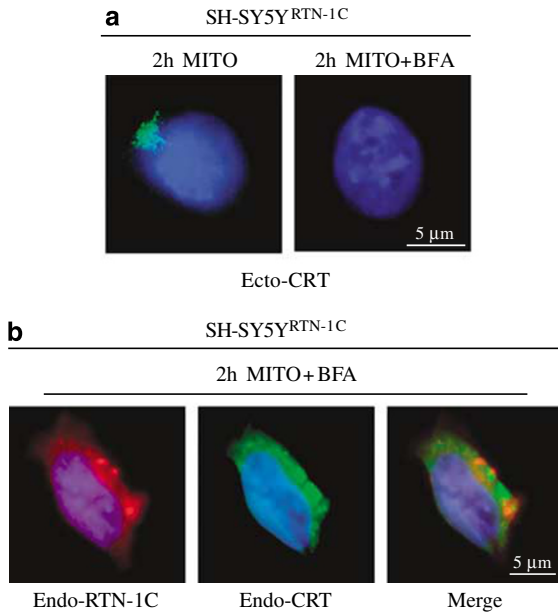
278

Figure 4 Brefeldin A-mediated suppression of the MITO-induced exposure of CRT on the cell surface. (a) Immunofluorescence labeling of ecto-CRT (green) in doxycycline-induced SH-SY5Y^{RTN-1C} cells treated with 1 μM MITO for 2 h in absence (on the left) and presence of 30 μM BFA (on the right). (b) Intracellular staining of CRT (green) and RTN-1C (red) in SH-SY5Y^{RTN-1C} cells after 2 h of 1 μM MITO and 30 μM BFA treatment. Nuclei were stained with DAPI (blue)

Figure 5 Effect of RTN-1C induction and MITO treatment on [Ca^{2+}]$_{ER}$ dynamics. (a) Representative [Ca^{2+}]$_{ER}$ measurements. SH-SY5Y^{RTN-1C} cells were infected with an adenovirus encoding an ER-targeted aequorin construct and then were left untreated or treated with 2 μg/ml doxycycline for 12–16 h. [Ca^{2+}]$_{ER}$ was measured as described in the Materials and Methods section. Cells were reconstituted with coelenterazine n in KRB containing no Ca^{2+} and 100 μM EGTA. Then, the cells were transferred to the perfusion chamber and refilling of ER was initiated by the addition of KRB containing 1 mM CaCl$_2$. Ca^{2+} leak was induced by the addition of 100 μM tBHQ. Representative traces from >10 experiments performed on four separate cell preparations are shown. (b) Effect of MITO on [Ca^{2+}]$_{ER}$ dynamics in control noninduced (−doxy) and RTN-1C-overexpressing cells (+doxy, SH-SY5Y^{RTN-1C}). [Ca^{2+}]$_{ER}$ was measured as in (a) and a group of cells was treated with 1 μM MITO for 2 h before measurement. The upper panel shows steady-state [Ca^{2+}]$_{ER}$. The middle panel depicts the velocity of initial Ca^{2+} influx, measured in the first 10 s after CaCl$_2$ addition. The lower panel shows the velocity of Ca^{2+} leak after SERCA inhibition by tBHQ, normalized to the steady-state [Ca^{2+}]$_{ER}$ level (mean ± S.E.M.; *P < 0.05, **P < 0.01)

handling apparatus in the same cellular model. Thus, we applied MITO (Figure 6a), the intracellular Ca^{2+} chelator 1,2-bis(2-aminophenoxy)ethane-N,N,N,N-tetracetate acetyloxy methylester (BAPTA-AM) (Figure 6b), and the expression of an ER-targeted IP$_3$ receptor ligand-binding domain (LBD) construct (ER-targeted IP$_3$ receptor ligand binding domain (ER-IP$_3$R-LBD)$_{224–605}$) that is known to reduce [Ca^{2+}]$_{ER}$ in HeLa cells[35,36] (Figure 6c). A significant depletion of the ER Ca^{2+} pool was observed in all cases, as reflected by the reduced steady-state [Ca^{2+}]$_{ER}$ values (Figure 6a–c upper panels). Interestingly, the tendency was similar to the effect of RTN-1C, that is, the steady-state [Ca^{2+}]$_{ER}$ was unbalanced by reduced ER filling (see Figure 6a–c middle panels). Next, we analyzed the effect of the aforementioned strategies on CRT exposure on the cell surface. Importantly, all manipulations induced some degree of CRT exposure (Control < MITO < BAPTA-AM < ER-IP$_3$R-LBD$_{224–605}$, Figure 6d and e). Moreover, these data were confirmed in the neuroblastoma cell model. In doxycycline-treated SH-SY5Y^{RTN-1C} (RTN-1C over-expressing) cells, the chelation of Ca^{2+} with BAPTA-AM strongly enhanced the MITO-induced CRT exposure with respect to SH-SY5Y^{Tet12} (control) cells (Figure 7). Based on these data, we concluded that Ca^{2+} is a major regulator of CRT translocation. In particular, it appears that the reduction of Ca^{2+} refilling into the ER from the extracellular space serves as a trigger for CRT translocation. It is important to note that none of these manipulations induced apoptosis within the time frame that was analyzed (2 h for MITO, BAPTA-AM, 24 h post-transfection for ER-IP$_3$R-LBD$_{224–605}$),
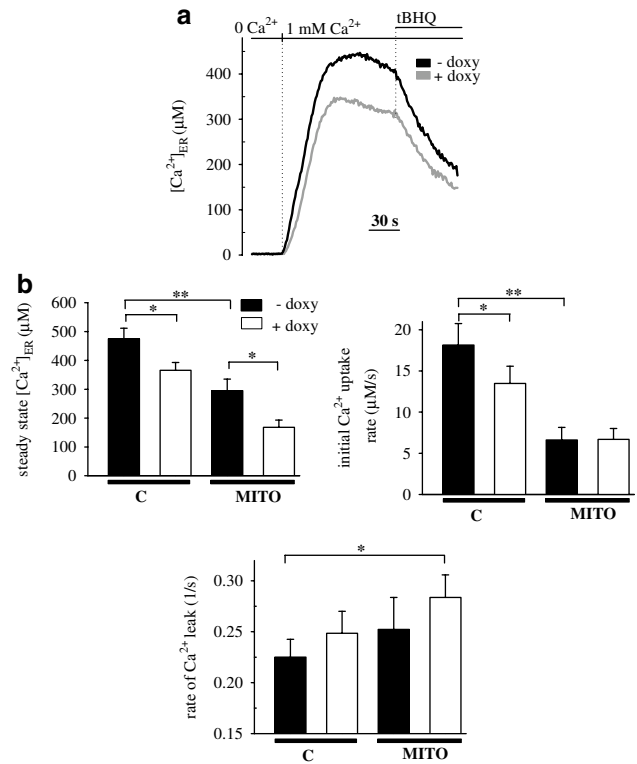
underscoring that CRT exposure is not directly linked to cell death.

The refilling of the ER after Ca^{2+} depletion was recently explained in mechanistic terms by the interaction of Ca^{2+} sensors residing in the ER membrane and store-operated Ca^{2+} channels of the PM (e.g. the Orai family of Ca^{2+} channels).[37,38] ER Ca^{2+} depletion triggers activation of Ca^{2+} influx through the PM, which is immediately taken up by the ER through the SERCA pumps.[32] To determine whether reduced ER refilling of RTN-1C-overexpressing cells reflects inhibition of Ca^{2+} influx through the PM, or inhibition of active transport into the ER lumen by the SERCA pumps, we applied two different approaches.

First, we measured the kinetics of Ca^{2+} uptake into the ER in cells in which the PM was permeabilized by a low dose of digitonin. Increasing the concentration of ATP (from 100 to
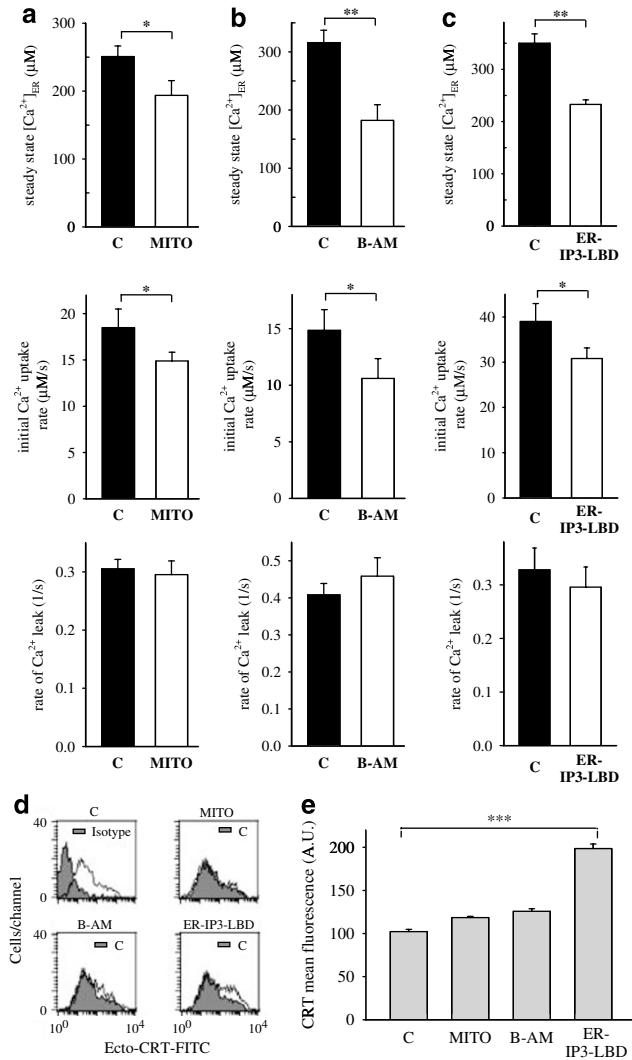
Figure 6 Induction of CRT exposure correlates with the reduction of $[Ca^{2+}]_{ER}$ levels. (**a**, **b**) Effect of MITO and BAPTA-AM treatment on $[Ca^{2+}]_{ER}$ dynamics in HeLa cells. HeLa cells were transfected with pcDNA1-er-AEQ construct and treated for 2 h with 1 μM MITO (**a**) or loaded with 10 μM BAPTA-AM (**b**) for 30 min before reconstitution with coelenterazine n. The dynamics $[Ca^{2+}]_{ER}$ were measured as in Figure 5. (**c**) Effect of the expression of an ER-targeted IP$_3$R ligand-binding domain (LBD) on $[Ca^{2+}]_{ER}$ dynamics in HeLa cells. Cells were transiently transfected with pcDNA1er-AEQ, together with ER targeted mRFP (monomeric Red Fluorescent Protein) (controls) or ER-IP$_3$R-LBD$_{224–605}$, tagged with mRFP. Results in (**a–c**) are means ± S.E.M. *$P<0.05$, **$P<0.01$. (**d**, **e**) Effect of MITO, BAPTA-AM, and ER-IP$_3$R-LBD$_{224–605}$ on CRT exposure. Cells were transfected with ER targeted-mRFP (control, C) or ER-IP$_3$R-LBD$_{224–605}$-mRFP for 24 h, treated with 1 μM MITO or 10 μM BAPTA-AM and analyzed for CRT exposure by FACS, limiting the CRT measurements on transfected (mRFP-expressing) and live (DAPI-negative) cells. Results of the quantitative analysis of CRT mean fluorescence are shown in (**e**) in arbitrary units (AU) and are the means ± S.E.M. of duplicate determinations from three independent experiments (***$P<0.005$)

Figure 7 Induction of CRT exposure by intracellular Ca^{2+} chelation. (**a**) SH-SY5Y^{Tet12} and RTN-1C-overexpressing SH-SY5Y^{RTN-1C} cells were treated for 30 min with 1 μM MITO or with 1 μM MITO after 30 min of pretreatment with 10 μM BAPTA-AM, and analyzed for the CRT exposure by cytofluorimetric immunodetection. (**b**) Quantitative analysis of ecto-CRT after incubation with the before mentioned agents. Data are the means (± S.E.M.) from three independent experiments and the CRT mean fluorescence is reported as percentage of control (in untreated cells)

400 μM) in the incubating medium augmented SERCA activity, as it was reflected by the increased Ca^{2+} filling rate of the ER. The overexpression of RTN-1C had no significant effect on SERCA activity (Figure 8a). These results suggest that putative interactions between RTN-1C and SERCA cannot account for the RTN-1C-facilitated CRT exposure. Next, in order to directly assess the effect of RTN-1C on Ca^{2+}
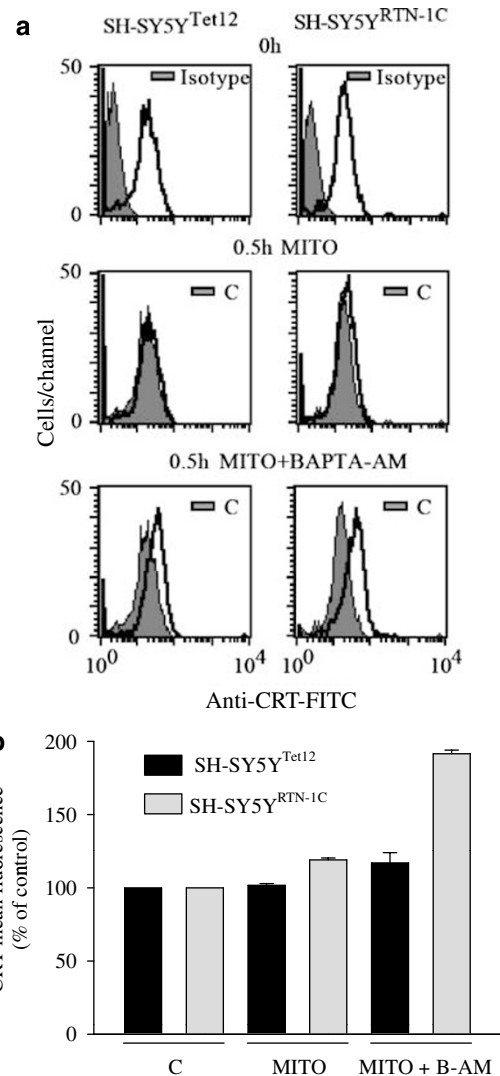
influx through the PM, we measured the kinetics of the increase of cytosolic $[Ca^{2+}]$ ($[Ca^{2+}]_c$) after induction of capacitative Ca^{2+} influx by ER Ca^{2+} depletion (Figure 8b). SH-SY5Y^{RTN-1C} cells with (RTN-1C overexpressing) or without (controls) doxycycline treatment were first perfused with Ca^{2+}-free Krebs Ringer-modified Buffer (KRB) containing 100 μM EGTA and then treated for 5 min with 50 μM tBHQ to deplete ER Ca^{2+} content. At last, Ca^{2+} influx was induced by the addition of 1 mM CaCl$_2$ to the KRB buffer while removing EGTA (Figure 8b, left panel). Importantly, RTN-1C overexpression significantly reduced the Ca^{2+} influx rate (Figure 8b, right panel), unraveling the molecular target by which home protein exerts its effect on Ca^{2+} refilling of the ER.
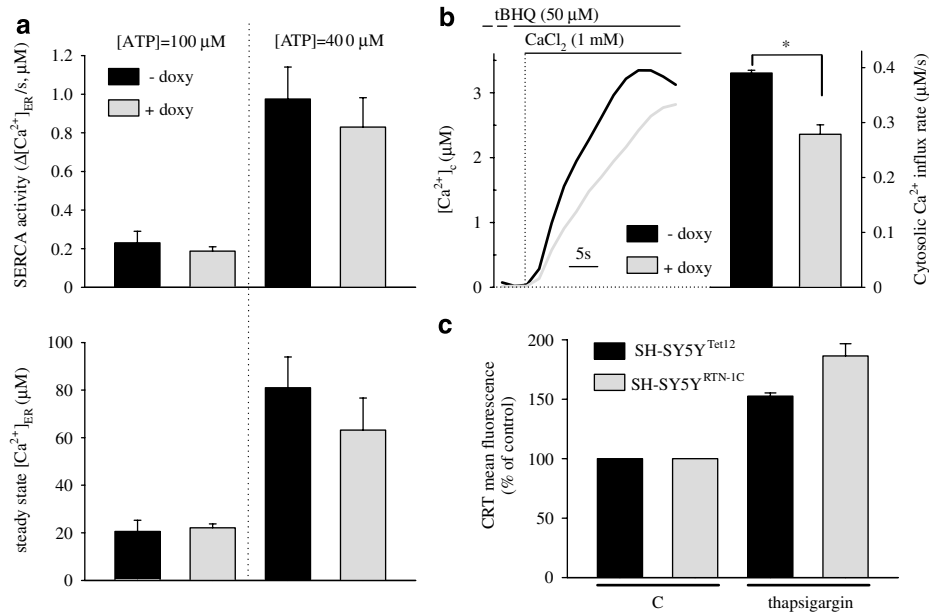
Figure 8 The role of SERCA activity in exposing CRT on the cell surface. (**a**) Measurement of Ca^{2+} uptake kinetics in digitonin-permeabilized SH-SY5Y^{RTN-1C} cells with or without induction with doxycycline. [Ca^{2+}]$_{ER}$ was measured in ad-er-AEQ-infected cells as described in Figure 5. After reconstitution and washing, cells were permeabilized with an intracellular solution (ICS) containing 25 μM digitonin and 0 Ca^{2+}. ER refilling was initiated by the addition of 200 nM free [Ca^{2+}], buffered by 2 mM EGTA and 2 mM HEDTA. Two different ICS were used containing 100 or 400 μM ATP. Initial Ca^{2+} uptake kinetics (upper panel, measured in the first 30 s of uptake) and steady-state [Ca^{2+}]$_{ER}$ (lower panel) are presented on the graphs. (**b**) Measurement of capacitative Ca^{2+} influx kinetics in SH-SY5Y^{RTN-1C} cells with or without doxycycline induction. [Ca^{2+}]$_c$ was measured in ad-cyt-AEQ-infected cells as described in Materials and Methods. Cells were first perfused with Ca^{2+}-free KRB containing 100 μM EGTA, then ER was Ca^{2+} depleted by 50 μM tBHQ (5 min). Finally, Ca^{2+} influx was induced by the addition of 1 mM CaCl$_2$ to the KRB buffer and removing EGTA. The left panel shows representative traces of control and doxycycline-induced SH-SY5Y^{RTN-1C} cells after Ca^{2+} addition. The right panel shows the mean ± S.E.M. of velocity of [Ca^{2+}] increase in the cytoplasm of the two experimental groups of cells. Results are from 15 traces from three independent experiments. *$P < 0.005$. (**c**) Effect of SERCA inhibition on CRT exposure in the cell surface. SH-SY5Y^{Tet12} and doxycycline-treated SH-SY5Y^{RTN-1C} cells were stimulated for 2 h with 10 μM thapsigargin and analyzed for CRT exposure by FACS analysis

In conclusion, we deciphered the complex mechanism by which RTN-1C modifies ER and cellular Ca^{2+} homeostasis. This mechanism includes actions both on the ER and the PM, in agreement with the double localization of the protein. Indeed, RTN-1C appears to increase Ca^{2+} leak from the ER lumen to the cytosol, accounting for elevated basal [Ca^{2+}]$_c$ as they were observed in doxycycline-treated SH-SY5Y^{RTN-1C} cells.[23] In addition, RTN-1C also inhibits capacitative Ca^{2+} influx at the PM level, further reducing the steady-state [Ca^{2+}] in the ER. Similarly, the effect of RTN-1C on CRT cell surface exposure cannot be accounted for by an effect on a single target. Thus, even though the reduction of ER Ca^{2+} refilling by RTN-1C was mediated by the inhibition of PM Ca^{2+} channels, inhibition of the SERCA pump by thapsigargin was also able to induce CRT exposure, and this effect was more evident in SH-SY5Y^{RTN-1C} cells following RTN-1C induction (Figure 8c). This suggests that any manipulation leading to [Ca^{2+}]$_{ER}$ depletion may stimulate CRT exposure, irrespective of the exact mechanism by which this depletion is achieved. Further experiments are needed to clarify the exact role of the individual components of ER Ca^{2+} homeostasis in generating the signal for triggering CRT exposure onto the cellular surface. Whether cell surface CRT itself modifies Ca^{2+} fluxes cannot be excluded, yet appears improbable because this protein has thus far been viewed as a mere Ca^{2+} buffer. Indeed, induction of CRT exposure with inhibitors of protein phosphatase 1 (PP1) failed to cause significant changes in

[Ca^{2+}]$_{ER}$ (not shown), underscoring that ecto-CRT by itself does not modulate Ca^{2+} fluxes.

Concluding Remarks

Based on the data summarized in this work, we assume that ER Ca^{2+} homeostasis plays a major role in the regulation of CRT exposure as it is induced by anthracyclins. Our data corroborate that anthracyclins can reduce the ER Ca^{2+} concentration.[17–19] Although statistically significant and consistent (in more than 15 independent experiments), this effect is far from spectacular, at least in SH-SY5Y neuroblastoma cells. Upon RTN-1C overexpression (which reduces ER Ca^{2+} influx and hence further lowers the [Ca^{2+}]$_{ER}$) or after treatment with the Ca^{2+} chelator BAPTA-AM (which also reduces ER Ca^{2+} influx), however, SH-SY5Y cells acquired the capacity to expose CRT in response to anthracyclins. These results suggest that threshold effects operating at the level of [Ca^{2+}]$_{ER}$ may determine the propensity of different cell types to translocate CRT to the cell surface. As a further indication that [Ca^{2+}]$_{ER}$ controls CRT exposure, we observed that two further specific manipulations designed to lower [Ca^{2+}]$_{ER}$ could stimulate the appearance of CRT on the cell surface: inhibition of SERCA pumps with thapsigargin and transfection with ER-IP$_3$R-LBD$_{224-605}$.

Although the before mentioned results clearly demonstrate that [Ca^{2+}]$_{ER}$ controls CRT exposure, several problems

remain to be resolved. First, it is not clear whether a reduction of [Ca^{2+}]$_{ER}$ levels is the sole mediator responsible for CRT exposure induced by an array of different stressors or whether alternative routes to stress-induced CRT exposure may exist. To answer this question, it will be necessary to screen an array of chemical or physical stressors for their effects on CRT exposure and [Ca^{2+}]$_{ER}$ levels. Second, the kinetics of CRT exposure and apoptosis induction proceeds at rather different paces. While CRT exposure elicited by anthracyclins is a rapid phenomenon (that manifests within minutes or few hours), apoptosis occurs much later (within > 12 h), raising questions on the functional relationship between the two phenomena. Indeed, transfection with ER-IP$_3$R-LBD$_{224-605}$ can stimulate CRT exposure. However, this manipulation does not trigger an apoptotic response, suggesting that CRT exposure and apoptosis induction can be uncoupled. Third, at present it remains unknown which pool of CRT translocates to the surface. Immunofluorescence experiments performed on permeabilized *versus* nonpermeabilized cells did not reveal a net reduction of intracellular CRT that would accompany the exposure of CRT on the surface. Thus, there is only a fraction of CRT that may translocate to the cell surface. The subcellular origin and the biochemical features of this ecto-CRT pool have to be determined. Fourth, the experiments shown here have been performed on human neuroblastoma and cervical cancer cells, which are not suitable for determining the immunological consequences of [Ca^{2+}]$_{ER}$-regulated CRT exposure. Thus, future studies performed on RTN-1C-expressing mouse tumor cells will have to confirm their enhanced CRT-dependent immunogenicity after *in vivo* treatment with anthracyclins.

We have recently reported that CRT exposure could be observed in a fraction of circulating leukemia cells from patients treated by intravenous injection with anthracyclins.[39] However, CRT exposure could not be found in all leukemias, pointing to a hitherto unsuspected heterogeneity in the mechanisms of CRT exposure. The mechanisms accounting for this deficient CRT exposure remain largely elusive, although they may be related to altered ER Ca^{2+} homeostasis. It is tempting to speculate that tumors that fail to expose CRT would be refractory to the immunological component of chemotherapy and hence would demonstrate a poorer prognosis than tumors that conserve an intact CRT translocation response. This possibility is currently under intense investigation in our laboratory.

Materials and Methods

Antibodies and reagents. The rabbit polyclonal (FMC 75) to calreticulin (ab2907) and the mouse monoclonal (RNL-4) to NSP-A + NSP-B (ab8961) antibodies were from Abcam. The mouse anti-actin monoclonal antibody was from AbCys S.A. The rabbit anticleaved caspase 3 was from Cell Signaling. Ionomycin, EGTA, bovine serum albumin (BSA), digitonin, CaCl$_2$ were from Sigma Aldrich. Mitoxanthrone, BFA, BAPTA-AM, thapsigargin were obtained from Calbiochem. Doxycycline was purchased by Clontech. Lipofectamine™ 2000 reagent, blasticidin S HCl and zeocin™ were from Invitrogen.

RTN-1C expression plasmid. The full length of human RTN-1C cDNA was subcloned into the Invitrogen (Carlsbad, CA, USA) pcDNA3.1/Zeo vector to generate the pcDNA 3.1/Zeo RTN-1C plasmid and confirmed by sequencing.

Cells, transfection, treatments. The stably transfected clones for RTN-1C sense were obtained as previously described.[23] The SH-SY5Y human neuroblastoma cell line and the derived clones were grown in 1 : 1 mixture of Dulbecco's modified Eagle's medium (DMEM) and Ham's F12 with Glutamax (GIBCO, Invitrogen) supplemented with 10% tetracycline-free heat-inactivated fetal bovine serum (FBS, Clontech) in a humidified atmosphere of 5% CO$_2$ in air under selective conditions by adding blasticidin and zeocin periodically. HeLa cells were maintained in DMEM supplemented with 10% heat-inactivated FBS, 10 mM Hepes, 100 U/ml penicillin, and 100 μg/ml streptomycin. For transfection of HeLa cells, 1×10^5 cells/well were seeded into 12-well plates and transfected 24 h later by each expression vector plasmid by using lipofectamine™ 2000 according to the manufacturer's instructions. All experiments in SH-SY5Y^{RTN-1C} were performed on cells after 12 h of induction by doxycycline (2 μg/μl).

Assessment of apoptosis. Redistribution of PM phosphatidylserine is a marker of apoptosis and was assessed by annexin fluorescein isothiocyanate (MACS, Miltenyi Biotech) according to the manufacturer's protocol. Briefly, 2×10^5 cells per sample were collected, washed in phosphate-buffered saline (PBS), pelleted, and resuspended in incubation buffer (10 mM HEPES/NaOH, pH 7.4, 140 mM NaCl, 5 mM CaCl$_2$) containing 1% annexin V. Samples were kept in the dark and incubated for 15 min prior to addition of another 400 μl of incubation buffer and subsequent analysis on a fluorescence-activated cell sorter Calibur flow cytometer (Becton Dickinson) using Cell Quest software.

Flow cytometric analysis of CRT and RTN-1C on the cell surface. Flow cytometry was used to detect CRT and RTN-1C exposure induced by different drugs. Briefly, 2×10^5 cells were plated in 12-well plates and the day after treated with different drugs for 2 h. Cells were harvested, washed twice with PBS and fixed in 0.25% paraformaldehyde (PFA) in PBS for 5 min. After washing again twice in cold PBS, cells were incubated for 30 min with primary antibody, diluted in cold blocking buffer (2% FBS in PBS), followed by washing and incubation with the FITC-conjugated monoclonal or polyclonal secondary antibody diluted 1:500 in blocking buffer (30 min). Each sample was then analyzed by FACScan (Becton Dickinson) to identify cell-surface CRT and RTN-1C. Isotype-matched IgG antibodies were used as a control, and the fluorescent intensity of stained cells was gated on propidium iodide (PI) or 4′,6-diamidino-2-phenylindole (DAPI)-negative cells. Data were recorded on a logarithmic scale and analyzed using Cell Quest software. Results are shown both as frequency histograms and, after quantification of mean fluorescence intensity values, also as fold induction in bar charts.

Immunofluorescence. For surface staining: cells were cultured on 13 mm-round glass coverslips as described above. After treatment, cells were placed on ice, washed twice with PBS and fixed in 0.25% PFA in PBS for 5 min. Cells were then washed twice in PBS and primary antibody, diluted in cold blocking buffer, was added for 30 min. After three washes in cold PBS, cells were incubated for 30 min with the appropriate secondary antibody diluted 1:500 in cold blocking buffer. Cells were washed with PBS and mounted on slides with the mounting medium including DAPI from Vectashield. For intracellular staining: cells were washed with PBS, fixed with 4% PFA for 15 min, permeabilized with 0.1% Triton X-100 for 10 min, rinsed three times with PBS, and nonspecific binding sites were blocked with 10% FBS in PBS for 30 min. Primary antibody was added for 1 h. Subsequently, cells were washed three times with PBS and incubated for 30 min in Alexa Fluor FITC or TRITC-conjugated secondary antibodies (1:1000, Molecular Probes). Specimens were imaged by a brightfield microscope coupled to a cooled CCD camera or a Zeiss LSM 510 confocal system.

Western blot analyses. Cells were harvested and homogenized in RIPA lysis buffer (10 mM Tris, pH 7.2, 150 mM NaCl, 1% deoxycholate, 1% Triton, 0.1% SDS, 5 mM EDTA) containing complete protease inhibitor cocktail (Roche Diagnostics, Meylan, France). After 1 h on ice, samples were sonicated and protein quantification was carried out using a Bio-Rad protein assay. Equal amounts of soluble proteins (15–25 μg) were denatured by boiling and resolved by sodium dodecyl sulfate-polyacrylamide gel electrophoresis (SDS-PAGE) and transferred to a nitrocellulose membrane. After blocking in 5% non-fat dry milk in PBS for 1 h and probing with a specific primary antibody and a horseradish peroxidase-conjugated secondary antibody, the protein bands were detected by chemiluminescence (Supersignal, Pierce) and X-ray film exposure (Kodak). Protein loading was normalized by using anti-tubulin or anti-actin antibodies.

Dynamic *in vivo* [Ca^{2+}] measurements. For [Ca^{2+}]$_{ER}$ measurements, HeLa cells were cotransfected with pcDNA1-er-AEQ and the appropriate cDNAs, or SH-SY5Y^{RTN-1C} cells were infected with an ad-er-AEQ adenoviral construct (kind gift of M Chami, INSERM U807, Paris). Cells were reconstituted with coelenterazine n, following ER Ca^{2+} depletion in a solution containing 0 [Ca^{2+}], 600 μM EGTA, 1 μM ionomycin, for 1 h at 4°C, as previously described.[35] Following reconstitution, cells were washed with KRB (Krebs–Ringer modified buffer: 135 mM NaCl, 5 mM KCl, 1 mM MgSO$_4$, 0.4 mM K$_2$HPO$_4$, 5.5 mM glucose, 20 mM HEPES, pH = 7.4) containing 1 mM EGTA and 2% BSA, and transferred to the perfusion chamber. Light signal was collected in a purpose-built luminometer and calibrated into [Ca^{2+}] values as previously described.[29] Ca^{2+} reuptake into ER was initiated by the addition of KRB containing 1 mM CaCl$_2$. Measurement of Ca^{2+} uptake into the ER in permeabilized cells was performed in a similar way except that, after the BSA washing step, cells were perfused with an intracellular-like solution containing 25 μM digitonin as previously described.[40] [Ca^{2+}] was kept controlled by the use of 2 mM EGTA and 2 mM HEDTA and free ionic concentrations were calculated with the Max-Chelator software.[41] [Mg^{2+}] was kept constant at 2 mM while [ATP] varied between 100 and 400 μM. Ca^{2+} uptake was initiated by the addition of 200 nM free [Ca^{2+}]. Cytosolic [Ca^{2+}] measurements were performed on cells infected with an adenoviral ad-cyt-AEQ vector as previously described.[29]

Statistical analyses. Statistical analyses were performed using the Student's *t*-test. A *P*-value of 0.05 was considered as significant. All data are reported as means ± S.E.M.

1. Casares N, Pequignot MO, Tesniere A, Ghiringhelli F, Roux S, Chaput N et al. Caspase-dependent immunogenicity of doxorubicin-induced tumor cell death. *J Exp Med* 2005; **202**: 1691–1701.
2. Zitvogel L, Casares N, Pequignot MO, Chaput N, Albert ML, Kroemer G. Immune response against dying tumor cells. *Adv Immunol* 2004; **84**: 131–179.
3. Obeid M, Tesniere A, Panaretakis T, Tufi R, Joza N, van Endert P et al. Ecto-calreticulin in immunogenic chemotherapy. *Immunol Rev* 2007; **220**: 22–34.
4. Obeid M, Panaretakis T, Joza N, Tufi R, Tesniere A, van Endert P et al. Calreticulin exposure is required for the immunogenicity of gamma-irradiation and UVC light-induced apoptosis. *Cell Death Differ* 2007; **14**: 1848–1850.
5. Obeid M, Tesniere A, Ghiringhelli F, Fimia GM, Apetoh L, Perfettini JL et al. Calreticulin exposure dictates the immunogenicity of cancer cell death. *Nat Med* 2007; **13**: 54–61.
6. Johnson S, Michalak M, Opas M, Eggleton P. The ins and outs of calreticulin: from the ER lumen to the extracellular space. *Trends Cell Biol* 2001; **11**: 122–129.
7. Michalak M, Corbett EF, Mesaeli N, Nakamura K, Opas M. Calreticulin: one protein, one gene, many functions. *Biochem J* 1999; **344** (Part 2): 281–292.
8. Gardai SJ, McPhillips KA, Frasch SC, Janssen WJ, Starefeldt A, Murphy-Ullrich JE et al. Cell-surface calreticulin initiates clearance of viable or apoptotic cells through trans-activation of LRP on the phagocyte. *Cell* 2005; **123**: 321–334.
9. Apetoh L, Ghriringhelli F, Tesniere A, Obeid M, Ortiz C, Criollo A et al. Toll-like receptor 4-dependent contribution of the immune system to anti-cancer chemo- and radiotherapy. *Nat Med* 2007; **4**: 65–70.
10. Srivastava PK. Heat shock protein-based novel immunotherapies. *Drug News Perspect* 2000; **13**: 517–522.
11. Franz S, Herrmann K, Fuhrnrohr B, Sheriff A, Frey B, Gaipl US et al. After shrinkage apoptotic cells expose internal membrane-derived epitopes on their plasma membranes. *Cell Death Differ* 2007; **14**: 733–742.
12. Kroemer G, Galluzzi L, Brenner C. Mitochondrial membrane permeabilization in cell death. *Physiol Rev* 2007; **87**: 99–163.
13. Maestre N, Tritton TR, Laurent G, Jaffrezou JP. Cell surface-directed interaction of anthracyclines leads to cytotoxicity and nuclear factor kappaB activation but not apoptosis signaling. *Cancer Res* 2001; **61**: 2558–2561.
14. Delpy E, Hatem SN, Andrieu N, de Vaumas C, Henaff M, Rucker-Martin C et al. Doxorubicin induces slow ceramide accumulation and late apoptosis in cultured adult rat ventricular myocytes. *Cardiovasc Res* 1999; **43**: 398–407.
15. Laurent G, Jaffrezo JP. Signaling pathways activated by daunorubicin. *Blood* 2001; **98**: 913–924.
16. Ravi D, Muniyappa H, Das KC. Endogenous thioredoxin is required for redox cycling of anthracyclines and p53-dependent apoptosis in cancer cells. *J Biol Chem* 2005; **280**: 40084–40096.
17. Kim DH, Landry AB, Lee YS, Katz AM. Doxorubicin-induced calcium release from cardiac sarcoplasmic reticulum vesicles. *J Mol Cell Cardiol* 1989; **21**: 433–436.
18. Takahashi S, Denvir MA, Harder L, Miller DJ, Cobbe SM, Kawakami M et al. Effects of *in vitro* and *in vivo* exposure to doxorubicin (adriamycin) on caffeine-induced Ca2+ release from sarcoplasmic reticulum and contractile protein function in 'chemically-skinned' rabbit ventricular trabeculae. *Jpn J Pharmacol* 1998; **76**: 405–413.
19. Kim E, Tam M, Siems WF, Kang C. Effects of drugs with muscle-related side effects and affinity for calsequestrin on the calcium regulatory function of sarcoplasmic reticulum microsomes. *Mol Pharmacol* 2005; **68**: 1708–1715.
20. Roebroek AJ, Contreras B, Pauli IG, Van de Ven WJ. cDNA cloning, genomic organization, and expression of the human RTN2 gene, a member of a gene family encoding reticulons. *Genomics* 1998; **51**: 98–106.
21. Grand T, Nakamura F, Vartanian T, Strittmatter SM. Identification of the Nogo inhibitor of axon regeneration as a reticulon protein. *Nature* 2000; **403**: 439–444.
22. Moreira EF, Jaworski CJ, Rodriguez IR. Cloning of a novel member of the reticulon gene family (RTN3): gene structure and chromosomal localization to 11q13. *Genomics* 1999; **58**: 73–81.
23. Di Sano F, Fazi B, Tufi R, Nardacci R, Piacentini M. Reticulon-1C acts as a molecular switch between endoplasmic reticulum stress and genotoxic cell death pathway in human neuroblastoma cells. *J Neurochem* 2007; **102**: 345–353.
24. Oertle T, Schwab ME. Nogo and its paRTNers. *Trends Cell Biol* 2003; **13**: 187–194.
25. van de Velde HJ, Roebroek AJ, Senden NH, Ramaekers FC, Van de Ven WJ. NSP-encoded reticulons, neuroendocrine proteins of a novel gene family associated with membranes of the endoplasmic reticulum. *J Cell Sci* 1994; **107**: 2403–2416.
26. Roebroek AJ, Ayoubi TA, Van de Velde HJ, Schoenmakers EF, Pauli IG, Van de Ven WJ. Genomic organization of the human NSP gene, prototype of a novel gene family encoding reticulons. *Genomics* 1996; **32**: 191–199.
27. Hens J, Nuydens R, Geerts H, Senden NH, Van de Ven WJ, Roebroek AJ et al. Neuronal differentiation is accompanied by NSP-C expression. *Cell Tissue Res* 1998; **292**: 229–237.
28. Demaurex N. Calcium measurements in organelles with Ca2+-sensitive fluorescent proteins. *Cell Calcium* 2005; **38**: 213–222.
29. Chiesa A, Rapizzi E, Tosello V, Pinton P, de Virgilio M, Fogarty KE et al. Recombinant aequorin and green fluorescent protein as valuable tools in the study of cell signalling. *Biochem J* 2001; **355**: 1–12.
30. Pinton P, Ferrari D, Rapizzi E, Di Virgilio F, Pozzan T, Rizzuto R. The Ca2+ concentration of the endoplasmic reticulum is a key determinant of ceramide-induced apoptosis: significance for the molecular mechanism of Bcl-2 action. *EMBO J* 2001; **20**: 2690–2701.
31. Parekh AB, Putney Jr JW. Store-operated calcium channels. *Physiol Rev* 2005; **85**: 757–810.
32. Jousset H, Frieden M, Demaurex N. STIM1 knockdown reveals that store-operated Ca2+ channels located close to sarco/endoplasmic Ca2+ ATPases (SERCA) pumps silently refill the endoplasmic reticulum. *J Biol Chem* 2007; **282**: 11456–11464.
33. Michalak M, Robert Parker JM, Opas M. Ca2+ signaling and calcium binding chaperones of the endoplasmic reticulum. *Cell Calcium* 2002; **32**: 269–278.
34. Williams DB. Beyond lectins: the calnexin/calreticulin chaperone system of the endoplasmic reticulum. *J Cell Sci* 2006; **119**: 615–623.
35. Szabadkai G, Bianchi K, Varnai P, De Stefani D, Wieckowski MR, Cavagna D et al. Chaperone-mediated coupling of endoplasmic reticulum and mitochondrial Ca2+ channels. *J Cell Biol* 2006; **175**: 901–911.
36. Varnai P, Balla A, Hunyady L, Balla T. Targeted expression of the inositol 1,4,5-triphosphate receptor (IP3R) ligand-binding domain releases Ca2+ via endogenous IP3R channels. *Proc Natl Acad Sci USA* 2005; **102**: 7859–7864.
37. Smyth JT, Dehaven WI, Jones BF, Mercer JC, Trebak M, Vazquez G et al. Emerging perspectives in store-operated Ca2+ entry: roles of Orai, Stim and TRP. *Biochim Biophys Acta* 2006; **1763**: 1147–1160.
38. Soboloff J, Spassova MA, Dziadek MA, Gill DL. Calcium signals mediated by STIM and Orai proteins – a new paradigm in inter-organelle communication. *Biochim Biophys Acta* 2006; **1763**: 1161–1168.
39. Chaput N, De Botton S, Obeid M, Apetoh L, Ghiringhelli F, Panaretakis T et al. Molecular determinants of immunogenic cell death: surface exposure of calreticulin makes the difference. *J Mol Med* 2007; **85**: 1069–1076.
40. Rapizzi E, Pinton P, Szabadkai G, Wieckowski MR, Vandecasteele G, Baird G et al. Recombinant expression of the voltage-dependent anion channel enhances the transfer of Ca2+ microdomains to mitochondria. *J Cell Biol* 2002; **159**: 613–624.
41. Patton C, Thompson S, Epel D. Some precautions in using chelators to buffer metals in biological solutions. *Cell Calcium* 2004; **35**: 427–431.

Supplementary Information accompanies the paper on Cell Death and Differentiation website (http://www.nature.com/cdd)